

Robust Geospatial Coordination of Multi-Agent Communications Networks Under Attrition

Jonathan S. Kent^{1,2,*}, Eliana Stefani³, Brian Plancher^{4,5}

Abstract—Coordinating emergency responses in extreme environments, such as wildfires, requires resilient and high-bandwidth communication backbones. While autonomous aerial swarms can establish ad-hoc networks to provide this connectivity, the high risk of individual node attrition in these settings often leads to network fragmentation and mission-critical downtime. To overcome this challenge, we introduce and formalize the problem of Robust Task Networking Under Attrition (RTNUA), which extends connectivity maintenance in multi-robot systems to explicitly address proactive redundancy and attrition recovery. We then introduce Physics-Informed Robust Employment of Multi-Agent Networks (Φ IREMAN), a topological algorithm leveraging physics-inspired potential fields to solve this problem. In our evaluations, Φ IREMAN consistently outperforms baselines, and is able to maintain greater than 99.9% task uptime despite substantial attrition in simulations with up to 100 tasks and 500 drones, demonstrating both effectiveness and scalability.

Index Terms—Multi-Robot Systems; Distributed Robot Systems; Aerial Systems; Applications

I. INTRODUCTION

IN large-scale emergency responses, such as urban or forest fires, responders are often distributed across multiple, shifting hotspots. Effective coordination in these scenarios relies on a constant flow of data between central command and the front lines. This problem is defined by a collection of dynamic tasks, each requiring a reliable communication backbone. However, infrastructure is frequently absent or compromised, and the high Size, Weight, and Power (SWaP) costs of satellite equipment often preclude its use [1]–[3]. A swarm of networking drones offers a viable alternative, autonomously organizing into an ad-hoc network to bridge this critical gap.

The environment in these scenarios is inherently hostile. Networking assets may undergo attrition, disabled by intense heat, smoke, or adversarial actions [4]. When a node fails, traditional systems react by repositioning remaining drones to re-establish connectivity. However, this reactive approach inevitably incurs *network downtime* during the transition, leaving responders isolated at critical moments. A truly robust system

must anticipate this attrition, possessing enough inherent redundancy to ensure that connectivity remains uninterrupted even as the network self-heals.

Beyond firefighting, these challenges are pervasive in disaster response [5], [6], search-and-rescue operations [4], [7], and tactical battlefield engagements [8], [9]. The common thread is the requirement for a self-healing architecture that maintains connectivity despite the loss of individual assets. While extensive research has explored task allocation [10]–[16], topology maintenance [17]–[21], spatial coordination [22], [23], and failure recovery [24]–[29] in isolation, few efforts have addressed the combined complexity of these challenges in a unified framework.

To overcome this challenge, this paper makes three primary contributions. First, we formalize the Robust Task-Networking Under Attrition (RTNUA) problem, integrating task allocation, topology maintenance, and attrition recovery with two new quantitative metrics. Second, we introduce Φ IREMAN, a physics-inspired framework that proactively generates redundant network geometries by utilizing potential fields to maintain a resilient mesh. Third, we provide an extensive evaluation across 25 configurations of problem size and attrition rate, demonstrating that Φ IREMAN consistently outperforms state-of-the-art baselines.

II. RELATED WORK

Related problems in multi-robot systems span task allocation, topology maintenance, spatial coordination, and failure recovery. However, existing literature rarely addresses the intersection of these domains required by the RTNUA problem.

Multi-Robot Task Allocation. While extensive MRTA literature addresses agent-to-task assignment [10]–[16], it largely treats communication as a secondary constraint rather than a spatial co-design problem [10], [30], failing to actively position agents to guarantee network connectivity.

Network Topology & Spatial Coordination. Approaches to multi-agent swarm topology generation [17]–[21] ensure connectivity but typically assume pre-allocated agents and crucially lack mechanisms to recover from attrition. Even joint MRTA-geometry solvers [21] remain static. Similarly, spatial coordination methods [22], [23] prioritize local collision avoidance and formation control over optimizing global communication topologies for task execution.

Robustness to Failures. Research on swarm attrition is predominantly reactive [31]–[33], focusing on task reassignment rather than network preservation. Other resilience strategies manage partial resource failures [26], adjust routes post-attrition [27], minimize future attrition risk [30], or model

Manuscript received: November, 19, 2025; Revised February, 25, 2025; Accepted March, 23, 2026.

This paper was recommended for publication by Editor M. Ani Hsieh upon evaluation of the Associate Editor and Reviewers' comments.

¹JSK is with Advanced Technology Center, Lockheed Martin Space, USA and Fu Foundation School of Engineering and Applied Science, Columbia University, New York, USA jonathan.s.kent@lmco.com

¹ES is with Lockheed Martin AI Center, Lockheed Martin Corporation, USA eliana.stefani@lmco.com

¹BP is with Barnard College, Columbia University, New York, USA and Dartmouth College, New Hampshire, USA plancher@dartmouth.edu
Digital Object Identifier (DOI): see top of this page.

Authors thank Columbia's Junfeng Yang, CMU's Katia Sycara, Wennie Tabib, UIUC's Indranil Gupta, Darci Peoples, TU Braunschweig's Dominik M. Krupke, Georgia Tech's Hazel B. Sparks.

Prior Work	Task Allocation	Topology Generation	Topology Maintenance	Spatial Coordination	Attrition Anticipation	Attrition Recovery
[2], [18]	✓	✓	✓	✓		✓
[10], [30]	✓				✓	
[19]			✓	✓	✓	
[21]	✓		✓	✓		
[22], [23]			✓	✓		
[24], [31], [32]	✓					✓
[25]	✓			✓		
[26]		✓	✓	✓		✓
[27]	✓		✓			✓
[28]	✓				✓	✓
[20] (MCCST)	✓		✓	✓		
[29] (DCCRS)	✓	✓	✓	✓	✓	✓
Ours	✓	✓	✓	✓	✓	✓

Table I: Feature sets and areas of concern for related work. Most works are not able to jointly handle task allocation and the generation and maintenance of network topologies in a geospatial setting, while anticipating and recovering from attrition based on features inherent in their design. Works are grouped according to features and concerns only, not on any basis of their operation. In later sections we demonstrate how our approach outperforms MCCST [20] and DCCRS [29] baselines.

fundamentally different combat dynamics [28], but none proactively configure networks to absorb the complete loss of agents.

Positioning Our Contribution. As summarized in Table I, only DCCRS [29] addresses the full scope of the RTNUA problem. However, DCCRS was designed strictly to retain network coherence under attrition, lacks explicit recovery mechanisms, and its evaluation ceases at the first instance of decoherence. Our approach extends physics-based swarm modeling [34]–[37] to actively organize drones into robust, self-healing network geometries. We evaluate these capabilities using the *TU1* and *TU2* metrics (introduced in Section III), which comprehensively capture network maintenance, recovery, and dispersion, including implementations of DCCRS and MCCST [20] as baselines for comparison.

III. ROBUST TASK NETWORKING UNDER ATTRITION

To enable precise algorithm development and systematic benchmarking, we formalize the RTNUA problem mathematically. The formalization captures three key requirements: drones must maintain network connectivity through spatial coordination, tasks require continuous connection to a base station, and random attrition degrades the network over time. We introduce two complementary metrics, *TU1* measuring overall task uptime and *TU2* discounting the dispersion phase, to evaluate algorithms comprehensively rather than simply measuring time-to-first-failure as in prior work.

A. Problem Formulation

An RTNUA problem is defined by a set of n drones $\mathcal{D} = \{D_1, D_2, \dots, D_n\}$ distributed spatially about \mathbb{R}^2 , with the base station controller B , with a communication radius R , at the origin. Each drone D_i is represented at time t by the tuple $D_i(t) = (\mathbf{x}_i(t), p_i, r_i, v_i, e_i(t), a_i(t))$, where:

- $\mathbf{x}_i(t) \in \mathbb{R}^2$ is the position relative to the base station
- $p_i(\delta t) \in [0, 1]$ is the probability of attrition in δt time
- $r_i \in \mathbb{R}_{>0}$ is its maximum communication radius
- $v_i \in \mathbb{R}_{>0}$ is its maximum speed
- $e_i(t) \in \{\text{TRUE}, \text{FALSE}\}$ is the current state of attrition, **FALSE** meaning it is alive and unattrited

- $a_i(t) \in \{\text{TRUE}, \text{FALSE}\}$ is the current activation state

In this model, two drones D_i, D_j can only communicate if $|\mathbf{x}_i - \mathbf{x}_j| \leq \min(r_i, r_j)$. For a given duration δt , each drone has the speed restriction $|\mathbf{x}_i(t + \delta t) - \mathbf{x}_i(t)| < v_i \delta t$. Drones start unattrited with $e_i(0) = \text{FALSE}$, and for duration δt , undergo attrition with probability $p_i(\delta t)$, such that $e_i(t + \delta t) = e_i(t) \vee \text{Bern}(p_i(\delta t))$. An attrited drone cannot be restored.¹ A drone is considered active if it is both unattrited and network-connected (either directly or indirectly):

$$a_i(t) = \neg e_i(t) \wedge (a_i^B(t) \vee a_i^d(t)), \quad (1)$$

where, $a_i^B(t) = |\mathbf{x}_i(t)| \leq \min(R, r_i)$, and $a_i^d(t) = (\exists D_j \in \mathcal{D} | a_j(t) \wedge |\mathbf{x}_i(t) - \mathbf{x}_j(t)| \leq \min(r_i, r_j))$.

The system includes m tasks $\mathcal{T} = \{T_1, T_2, \dots, T_m\}$. Practically speaking, each task would be an agent or set of agents requiring network connectivity, e.g. a group of firefighters, a member of the infantry, an unmanned ground vehicle, etc. Each task is represented as $T_i(t) = (\mathbf{y}_i(t), A_i(t))$, with position $\mathbf{y}_i(t) \in \mathbb{R}^2$ and connection state $A_i(t) \in \{\text{TRUE}, \text{FALSE}\}$. A task is connected if at least one active drone is in range:

$$A_i(t) = \exists D_j \in \mathcal{D} | a_j(t) \wedge |\mathbf{y}_i(t) - \mathbf{x}_j(t)| < r_j. \quad (2)$$

Denoting these as “tasks” is intended to stay in line with [19]–[21], and they equate to “leader drones” from [29].

A controller \mathcal{C} receives the set of networked drones $\mathcal{D}'(t) = \{D_i \in \mathcal{D} | a_i(t)\}$ and all tasks \mathcal{T} , providing motion instructions $\delta \mathbf{X}(t) = \{\delta \mathbf{x}_i(t)\}$ bounded by $|\delta \mathbf{x}_i(t)| \leq v_i$. For networked drones, $\mathbf{x}_i(t + \delta t) = \mathbf{x}_i(t) + \delta t \delta \mathbf{x}_i(t)$. For experimental purposes, we include a default behavior wherein unattrited but disconnected drones move directly toward the base station at constant speed until reconnected or destroyed, again leaving further development in this area to future work.

B. Objective Functions for Solution Benchmarking

The objective functions for RTNUA are closely related to established metrics from multi-robot systems and net-

¹This model of attrition was selected for computational simplicity, and more complex or geographically localized attrition can be treated in future work.

work algorithm literature. Network uptime ratios, expressed as $U = (T_{\text{operational}}/\tau)$, have been widely used to quantify system reliability in surveillance and monitoring applications. Similarly, temporal connectivity measures such as connectivity persistence $CP = (1/\tau) \int_0^\tau a(t)dt$, where $a(t)$ indicates connectivity at time t , provide mathematical frameworks for evaluating time-varying network performance [38], [39].

Building on these foundations, we define the primary objective to maximize expected task uptime:

$$TU1 = \mathbb{E}_{\text{scenario}} \left[\int_{t=0}^{\tau} \frac{1}{m} \sum_{T_i \in \mathcal{T}} A_i(t) dt \right] \quad (3)$$

This formulation provides an appropriate communication uptime metric for the multi-task setting, generalizing the proportion of time that communication links remain active to the average connectivity across all tasks, such that a task is connected if it is within range of an active networked drone. The metric aligns with coverage quality metrics in wireless sensor networks that employ temporal coverage quality $\int_0^\tau C(t)dt$ where $C(t)$ represents the coverage function [40], [41].

A secondary objective accounts for the speed of dispersion by only considering tasks after initial connection:

$$TU2 = \mathbb{E}_{\text{scenario}} \left[\int_{t=0}^{\tau} \frac{\sum_{T_i \in \mathcal{T}} A_i(t) dt}{\sum_{T_i \in \mathcal{T}} \exists t' \in [0, t] | A_i(t')} \right] \quad (4)$$

This metric is related to the monitoring coverage ratios used in persistent surveillance literature, particularly in connectivity-constrained multi-robot persistent surveillance frameworks where robots must visit sensing locations periodically while maintaining network connectivity [42]. The normalization by discovered tasks reflects similar approaches in multi-UAV cooperative systems where performance metrics account for the proportion of targets under surveillance throughout the mission [43], [44]. By providing this second metric, we can consider an algorithm's ability to maintain network uptime both in the context of and discounting its speed of dispersion.

The metric used in [29], introducing DCCRS, was only the length of time until network decoherence first occurs. While this is meaningful for the problem of faultless network maintenance, it does not capture any information about the severity of failures, the magnitudes of their effects on users of the network, or how well the system might recover from failures afterwards. Our formulations are intended to capture these and other challenges of maintaining robust network connectivity despite ongoing attrition, while allowing for practical constraints like limited communication ranges and drone velocities.

IV. Φ IREMAN ALGORITHM

The RTNUA formulation in Section III requires that a solution simultaneously allocates drones to tasks, generates and maintains a network topology connecting those tasks to the base station, and both anticipates and recovers from ongoing attrition, all while maximizing the time-averaged task connectivity captured by $TU1$ and $TU2$. Because these metrics penalize even brief connectivity interruptions across all tasks,

an effective algorithm must not only react to attrition after it occurs, but also proactively establish redundant network geometries that can absorb individual failures without disconnecting any task. To address these requirements, we developed the Physics-Informed Robust Employment of Multi-Agent Networks, or Φ IREMAN, algorithm, which leverages physics-inspired local interactions to achieve the desired robustness properties as emergent behaviors without requiring complex learning algorithms or extensive inter-agent communication.

The core insight underlying Φ IREMAN is that the topological properties of efficient sphere packings in two dimensions, i.e., that they spontaneously generate hexagonal meshes in low-energy configurations, naturally provide the path redundancy needed to sustain $TU1$ and $TU2$ under attrition, as any individual node in a hexagonal mesh may be removed without disconnecting its neighbors. By combining a task-space potential field, designed to guide drones toward an appropriate network geometry, with synthetic attractive and repulsive forces akin to those observed in polar fluids at the molecular level, we engineer an energy manifold whose low-energy states correspond to the drone network occupying the designed backbone geometry while generating and regenerating a hexagonal mesh pattern around it. Driving the system toward these low-energy states via gradient descent, we observe that task-directed dispersion, network contiguity, robustness to attrition, and recovery from connectivity loss all manifest as emergent behaviors, serving the $TU1$ and $TU2$ objectives without requiring explicit optimization against them.

A. The Computational Difficulties of Solving RTNUA

Calculating the expected uptime of tasks under the RTNUA formulation presents significant computational challenges due to the fundamental intractability of percolation theory in continuum systems. Unlike discrete lattice percolation with some exact solutions for specific cases [45], continuum percolation systems lack general analytical solutions [46], [47] and require computationally intensive Monte Carlo simulations [48], making direct optimization approaches prohibitively expensive for real-time use. While decentralized multi-agent reinforcement learning (MARL) offers a general approach to distributed decision-making, robust MARL systems require extensive offline training [49], significant inter-agent communication overhead scaling quadratically with agent count [50], and substantial computational resources unsuitable for resource-constrained edge devices [51]. This motivates the development of Φ IREMAN as a computationally efficient baseline that leverages physics-inspired local interactions to achieve emergent robustness without requiring complex learning algorithms or extensive inter-agent communication, and is further differentiated from DCCRS [29] by leveraging a Steiner tree approximation instead of velocity matching and leader following behaviors.

B. Task-Space Potential Field

We develop the geometric structure underlying the task space potential field by first constructing a graph that connects tasks to the base station. The potential at any location is then given

by its distance to the nearest point on this graph. While a minimal spanning tree would minimize total edge length, it can produce geometries that are detrimental to robustness, e.g. in the event that tasks form a horseshoe-shape with the base station located at one end, this would produce a geometry that would result in disconnection of the opposite end given an individual failure at any point (Figure 1, center and right).

Instead, we jointly minimize the total graph length l_{Σ_e} and the sum of path distances from tasks to base station l_{Σ_b} . The latter objective encourages more direct routes, reducing potential single points of failure. Additionally, since this is a geometric rather than purely topological problem, we greedily approximate a Steiner tree, inserting auxiliary Steiner nodes to reduce overall distance costs. The weighting coefficient c_b controls the trade-off between minimizing edge length and minimizing distances to base station. Higher values of c_b produce more direct routes at the cost of increased total edge length. Figure 1, left depicts a Semi-Steiner task tree.

C. Swarm Dynamics

Rather than explicitly simulating fluid dynamics with momentum, we use gradient descent on an energy manifold to drive drones toward low-energy configurations. This replicates the desired fluid-like behaviors more efficiently in both computation and motion. The total potential energy for drone D_i is given by the following, where $\mathbb{P} \cdot h^T(\mathbf{x}_i)$ represents the potential due to the task space potential field geometry, \mathcal{M} represents the attraction between drones, and P represents elastic repulsion between drones when closer than $q_i + q_j$:

$$E_i^\Sigma = E_i^p + E_i^{\mathcal{M}} + E_i^P, \quad \text{where :}$$

$$E_i^p = \mathbb{P} \cdot h^T(\mathbf{x}_i), \quad E_i^{\mathcal{M}} = \mathcal{M} \cdot \sum_{D_j \in \mathcal{D} | i \neq j} \frac{-1}{|\mathbf{x}_j - \mathbf{x}_i|}, \quad (5)$$

$$E_i^P = \frac{P}{2} \cdot \sum_{D_j \in \mathcal{D}'} (q_i + q_j - |\mathbf{x}_i - \mathbf{x}_j|)^2.$$

We note that \mathcal{D}' in the P term enumerates drones within repulsion range and q_i is nominally set to $r_i/2$ such that repulsion activates within communication range.

At each timestep, the controller \mathcal{C} performs multiple steps of gradient descent on the total energy $\mathcal{E}(t, \delta \mathbf{X}(t)) = \sum_{D_i \in \mathcal{D}'(t)} E_i^\Sigma$ to generate motion instructions $\delta \mathbf{X}(t)$. Descent terminates when equilibrium is reached, maximum steps are taken, or any instruction would exceed drone speed limits. Motion instructions are then executed, with drones that have undergone attrition ceasing all movement.

While gradient-based methods are susceptible to local minima, in the context of our swarm geometry, these minima represent stable, force-balanced configurations that fulfill the task-tree requirements. Because the energy landscape is dynamic, especially as drones move and undergo attrition, the system naturally explores the state space. Our analysis suggests that the current optimization approach generates sufficient topologies without the need for computationally expensive global search heuristics, as they effectively maximize the task uptime metrics as shown in Section V.

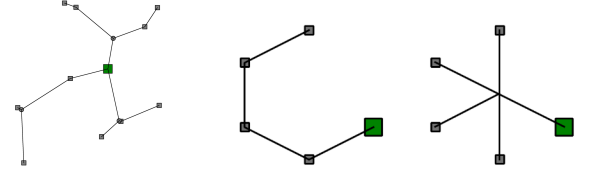


Figure 1: Left: Semi-Steiner task tree example with $c_b = 0.3$, balancing total edge length ($l_{\Sigma_e} = 19.86$) against sum of distances to base station ($l_{\Sigma_b} = 39.53$). Steiner nodes (circles) enable more efficient network topologies. Center: hypothetical task tree graph using only sum of distances. Right: task tree graph including sum of distances to base station.

D. Network Maintenance

As tasks move, Steiner node locations are continuously recalculated as the Fermat points of their three neighboring nodes. The complete task tree topology is periodically recomputed, with the new topology accepted if $l_{\Sigma}^{\text{new}} < \nu \cdot l_{\Sigma}^{\text{curr}}$, where $\nu \in (0, 1]$ is a threshold coefficient and $l_{\Sigma} = l_{\Sigma_e} + c_b \cdot l_{\Sigma_b}$.

Reaction to drone attrition requires no further extension. The potential field naturally causes neighboring drones to flow into gaps left by attrited agents, preserving network connectivity. The redundancy inherent in the hexagonal packing means that a limited number of losses can be absorbed without disruption.

E. Asynchronicity and Message Passing

To better reflect the constraints of practical deployments, we implement an asynchronous message-passing protocol to support a hybrid distributed-centralized architecture. Each agent maintains its own state and broadcasts it to its immediate neighbors, who receive the data in the subsequent timestep. While recursively forwarding information, agents retain only the most recent data based on timestamps and discard data that exceeds established temporal or spatial thresholds. While kinematic decisions and neighbor-coordination are computed locally, the high-level topological framework, that is the Semi-Steiner tree, is generated by a central base station with synchronous task-location data. This global topology is then propagated through the swarm using the same recursive forwarding logic. This hybrid approach allows drones to operate autonomously using local tree copies and navigate toward the base station to resynchronize if network contact is lost.

V. EXPERIMENTAL EVALUATION

A. Baseline Performance

We evaluate Φ IREMAN using a simulated environment with the following default configuration of both the underlying RTNVA problem and Φ IREMAN algorithm, using parameters determined via a grid search:

- 10 tasks uniformly distributed in $[-5, 5] \times [-5, 5] \subset \mathbb{R}^2$
- Base station at origin $(0, 0)$
- 50 drones initialized in a radius-1 ring about the base station with Gaussian noise ($\sigma = 0.2$)
- Communication radius $r_i = 2$, repulsion radius $q_i = 1$

- Maximum drone speed $v_i = 0.15$, with a probability of attrition per-simulation step of 1%
- Tasks random walk with Gaussian noise ($\sigma = 0.1$)
- Scenario length of 200 timesteps
- Task distance cost $c_b = 1.0$, topology threshold $\nu = 0.99$
- Potential field coefficients: attraction $\mathcal{M} = 0.05$, repulsion $P = 0.3$, task potential $\mathbb{P} = 0.05$

Φ IREMAN achieves task uptimes of $TU1 = 80.83\%$ and $TU2 = 85.34\%$. While this may appear modest compared to traditional network uptime metrics, it is achieved under substantial attrition with no computationally explicit recovery mechanism. Figure 3 shows the drone network evolution at $t = 0, 40, 80, 120, 160, 200$ timesteps. We note that this default setting is challenging, as on larger problem sizes that we explore shortly in our baseline comparisons, dispersion-discounted task uptime, $TU2$, exceeds 99.9%, even with substantial attrition.

B. Comparison Against Baselines

To explore the relationship between algorithmic performance, problem size, and attrition rate, we provide comparisons between Φ IREMAN and two baselines, DCCRS [29], and MCCST [20], over five problem sizes and five attrition rates, for a total of 25 configurations. Problem size definitions are provided in Table II.

For our implementation of DCCRS, hyperparameters with equivalents in Φ IREMAN were set to identical values, with all remaining hyperparameters determined via grid search for the default small, 1% attrition rate setting, and held constant across other configurations.

For our implementation of MCCST, to present the most faithful comparison possible to existing algorithms that include centralized components requiring synchronicity, drones were allowed to “cheat” by having perfect, instantaneous knowledge of the internal states of all other drones. A similar grid search approach was used to select hyperparameter values.

We simulated 100 different scenarios for each configuration, with identical scenarios run against all three algorithms by means of seeded random number generation, for a total of 7,500 simulations. Results are shown graphically as heatmaps in Figure 4 and in Table IV.

These results show strong and consistent outperformance by Φ IREMAN over both DCCRS and MCCST. Of the 25 configurations, Φ IREMAN is statistically significantly better than both DCCRS and MCCST in 13 configurations for $TU1$ and in 10 configurations for $TU2$, and is statistically significantly outperformed only once. Φ IREMAN demonstrates a maximum improvement against both baselines of 7.18 percentage points of $TU1$ in the extra small problem size with an attrition rate of 2%, being statistically significantly outperformed for the only time, by our “cheating” implementation of MCCST, with a performance deficit of 1.75 percentage points of $TU2$ in the medium problem size with an attrition rate of 5%. Elsewhere, Φ IREMAN outperforms MCCST by a maximum of 24.76 percentage points of $TU1$ in the small problem size with an attrition rate of 1%.

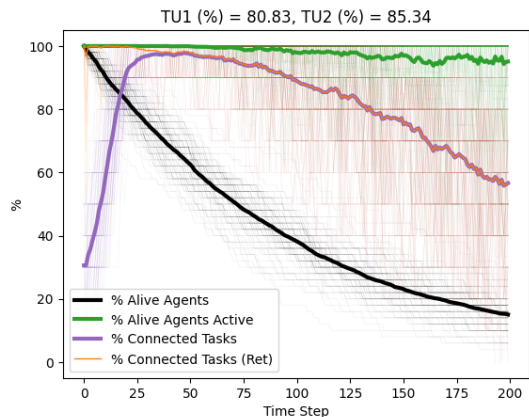


Figure 2: Performance over time of Φ IREMAN under the default configuration. Thick lines give per-timestep averages over 100 simulations. “Alive Agents” shows how many drone agents remain alive; “Alive Agents Active” shows the portion of alive agents which are networked; “Connected Tasks” shows how many tasks are connected; and “Connected Tasks (Ret)” shows how many of the previously connected tasks are currently connected. Once all tasks are connected for the first time, these last two overlap. The integral of the former is $TU1$, and the integral of the latter is $TU2$.

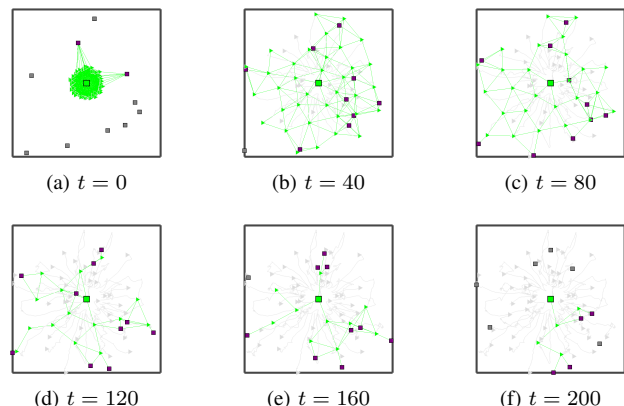


Figure 3: Evolution of drone network under default configurations at $t = 0, 40, 80, 120, 160, 200$ timesteps. Alive drones (green triangles when active, red when disconnected) maintain connectivity between tasks (purple squares when networked, gray when disconnected) and base station (green square) despite ongoing attrition (gray triangles). The gray square is the field border. Green lines are network connections.

C. Ablation Studies

We additionally conduct ablation studies to analyze the impact of each algorithm and simulation component, with results presented in Table III. All ablations are done in the context of the default configurations presented in Section V-A. These ablation studies suggest that Φ IREMAN performs robustly across problem parameters, and that problem size and attrition rate have dominating effects on performance, as expected.

1) *Task Graph Components*: Removing the task-space potential field entirely ($\mathbb{P} = 0$) reduces performance to $TU1 = 75.76\%$, $TU2 = 80.79\%$. While drones form efficient

Table II: Problem sizes for comparison studies.

Problem Size	Drones	Tasks	Field
XS	20	5	$[-2, 2] \times [-2, 2]$
S	50	10	$[-5, 5] \times [-5, 5]$
M	100	20	$[-10, 10] \times [-10, 10]$
L	200	50	$[-20, 20] \times [-20, 20]$
XL	500	100	$[-50, 50] \times [-50, 50]$

hexagonal patterns with near-perfect inter-drone connectivity, task uptime suffers from lack of guidance toward task positions. A similar yet slightly worse degradation to $TU1 = 75.21\%$, $TU2 = 80.16\%$ occurs when the edges of the Semi-Steiner tree are removed from the task-space potential field, as drones tend to form clusters around tasks and do not receive stimulus to form a network between them.

2) *Environmental Factors*: Decreasing the drone speed to $v_i = 0.1$ reduces $TU1$ to 78.45% while increasing the speed to $v_i = 0.2$ increases $TU1$ to 82.06%. In both cases, $TU2$ remains largely unchanged from the default, and only the $TU1$ reduction at $v_i = 0.1$ is statistically significant. This indicates that speed changes of this magnitude under these conditions primarily affect dispersion, and are of limited impact. Changing the standard deviation of the random walks of the tasks to $\sigma = 0$, rendering the tasks immobile, has no statistically significant effect, and neither does doubling task walk speed to $\sigma = 0.2$. While the motion of tasks relative to the field and the existing drone network might be a source of dispersion noise that helps the system escape unstable equilibria in theory, we find it to be statistically negligible.

VI. CONCLUSION AND FUTURE WORK

This paper introduces and formalizes the Robust Task Networking Under Attrition (RTNUA) problem and presents Φ IREMAN (Physics-Informed Robust Employment of Multi-Agent Networks), which achieves robust networking through physics-inspired fluid-like potential field dynamics, producing emergent behaviors that both anticipate and respond to attrition. Our experimental results demonstrate that Φ IREMAN successfully produces redundant network topologies that maintain connectivity despite ongoing attrition, outperforming state-of-the-art baselines. Problem size and attrition rate emerge as primary constraints on achievable task uptime, with the task-tree potential field geometry proving essential for guiding drones toward effective network configurations.

Several promising directions remain for future work. To focus on formalizing RTNUA and establishing Φ IREMAN's theoretical foundation, the present work restricts analysis to two-dimensional environments with uniformly distributed, randomly walking tasks, providing general results without application-specific assumptions. Future work may extend Φ IREMAN to 3D or incorporate task motion prediction for increased deployed performance. Future work could also explore large-scale multi-agent reinforcement learning approaches, which more directly optimize swarm performance against uptime [52]–[54]. Finally, hardware demonstrations in field scenarios, paired with improved underlying local control [55], [56], would validate the algorithm's real-world effectiveness in distributed settings.

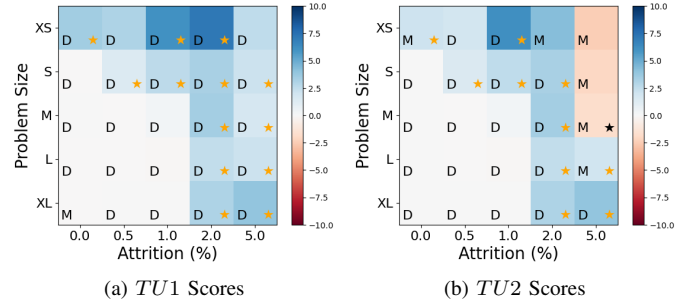


Figure 4: Heatmap of differences in $TU1$ and $TU2$ scores between Φ IREMAN, DCCRS, and MCCST across problem configurations. Values shown are the difference of the mean $TU1$ and $TU2$ scores of Φ IREMAN from the greater of DCCRS (D) or MCCST (M). Gold stars indicate that Φ IREMAN outperformed both baselines to a degree statistically significant at the $p < 0.05$ level. Black stars indicate that one of the baselines similarly outperformed Φ IREMAN. Overall, Φ IREMAN statistically significantly outperforms baselines in 46% of tests, is indistinguishable with scores over 95% in 38% of tests, and only statistically significantly lags baselines once.

Table III: Ablation study of algorithm components and environmental parameters on task uptime scores. Scores statistically significantly below the default configuration (at the $p < 0.05$ level) are italicized, while scores not statistically significantly different from the default are shown in default text. No scores statistically significantly above the default were found, confirming the validity of our results against ablation.

	Configuration	$TU1$ (%)	$TU2$ (%)
		Default	80.83
Task Graph	$P = 0$	<i>75.76 ± 1.84</i>	<i>80.79 ± 1.66</i>
	Nodes only	<i>75.21 ± 1.67</i>	<i>80.16 ± 1.52</i>
Environmental Factors	$v_i = 0.1$	<i>78.45 ± 1.69</i>	85.30 ± 1.44
	$v_i = 0.2$	82.06 ± 1.56	85.64 ± 1.47
	$\sigma = 0$	80.37 ± 1.81	85.11 ± 1.61
	$\sigma = 0.2$	80.18 ± 1.47	84.48 ± 1.39

REFERENCES

- [1] M. S. Couceiro, D. Portugal, J. F. Ferreira, and R. P. Rocha, "Semfire: Towards a new generation of forestry maintenance multi-robot systems," in *2019 IEEE/SICE International Symposium on System Integration (SII)*, 2019, pp. 270–276.
- [2] J. Hu, H. Niu, J. Carrasco, B. Lennox, and F. Arvin, "Fault-tolerant cooperative navigation of networked uav swarms for forest fire monitoring," *Aerospace Science and Technology*, vol. 123, p. 107494, 2022.
- [3] R. D. Arnold, H. Yamaguchi, and T. Tanaka, "Search and rescue with autonomous flying robots through behavior-based cooperative intelligence," *Journal of International Humanitarian Action*, vol. 3, no. 1, pp. 1–18, 2018.
- [4] F. Maresca, A. Romero, C. Delgado, V. Sciancalepore, J. Paradells, and X. Costa-Pérez, "React: Multi robot energy-aware orchestrator for indoor search and rescue critical tasks," 2025. [Online]. Available: <https://arxiv.org/abs/2503.05904>
- [5] J. P. Queraltá, J. Taipalmaa, B. Can Pullinen, V. K. Sarker, T. Nguyen Gia, H. Tenhunen, M. Gabbouj, J. Raitoharju, and T. Westerlund, "Collaborative multi-robot search and rescue: Planning, coordination, perception, and active vision," *IEEE Access*, vol. 8, pp. 191 617–191 643, 2020.
- [6] Z. Ning, Y. Yang, X. Wang, Q. Song, L. Guo, and A. Jamalipour, "Multi-agent deep reinforcement learning based uav trajectory optimization for differentiated services," *IEEE Transactions on Mobile Computing*, vol. 23, no. 5, p. 5818–5834, May 2024. [Online]. Available: <https://doi.org/10.1109/TMC.2023.3312276>

Table IV: We report $TU1$ and $TU2$ percentage scores for Φ IREMAN, DCCRS, and MCCST across various configurations, including 95% confidence intervals about the mean. For each configuration, $TU1$ and $TU2$ scores are analyzed independently. The top-performing algorithm is bolded only when its lead over all competitors is statistically significant at the $p < 0.05$ level according to a single-tailed Student's t -test. Φ IREMAN demonstrates meaningfully improved performance, statistically significantly outperforming both DCCRS and MCCST in 13 configurations for $TU1$ and 10 for $TU2$. Additionally, DCCRS achieves a score of greater than 95% in 9 of the remaining 12 configurations for $TU1$, and 99% in 9 of the remaining 15 configurations for $TU2$, greatly limiting the degree to which further improvements are possible. Φ IREMAN was significantly outperformed only once, by MCCST on $TU2$ in the medium problem size with 5% attrition, noting the caveat that our implementation of MCCST is permitted to “cheat” with all agents having instantaneous knowledge of the rest of the network.

Configuration		Φ IREMAN		DCCRS		MCCST	
Size	Attrition (%)	TU1	TU2	TU1	TU2	TU1	TU2
XS	0.0	92.79 \pm 0.98	98.69 \pm 0.48	89.32 \pm 1.65	96.46 \pm 1.01	84.59 \pm 1.75	96.58 \pm 0.99
	0.5	79.73 \pm 2.62	86.97 \pm 2.25	76.66 \pm 2.98	85.11 \pm 2.44	56.79 \pm 3.84	70.04 \pm 3.54
	1.0	61.63 \pm 3.14	70.51 \pm 3.05	55.58 \pm 3.55	64.37 \pm 3.25	42.49 \pm 3.24	57.12 \pm 3.37
	2.0	38.96 \pm 3.43	48.60 \pm 3.48	31.78 \pm 3.10	41.70 \pm 3.09	29.10 \pm 3.32	44.37 \pm 3.67
	5.0	21.54 \pm 2.64	32.64 \pm 3.08	19.00 \pm 2.47	30.48 \pm 3.09	18.17 \pm 2.91	35.13 \pm 4.25
S	0.0	95.62 \pm 0.26	99.95 \pm 0.02	95.66 \pm 0.27	99.91 \pm 0.09	89.03 \pm 0.77	98.66 \pm 0.37
	0.5	93.86 \pm 0.57	98.22 \pm 0.42	92.47 \pm 0.63	96.78 \pm 0.52	74.57 \pm 2.30	85.49 \pm 2.10
	1.0	80.83 \pm 1.63	85.34 \pm 1.51	78.21 \pm 1.84	82.78 \pm 1.66	56.07 \pm 2.84	68.18 \pm 2.66
	2.0	52.39 \pm 2.28	57.59 \pm 2.05	49.12 \pm 2.27	54.32 \pm 2.09	36.58 \pm 2.36	49.48 \pm 2.14
	5.0	25.57 \pm 1.69	32.93 \pm 1.57	23.39 \pm 1.83	31.03 \pm 1.91	20.42 \pm 1.79	34.99 \pm 2.03
M	0.0	95.96 \pm 0.17	99.98 \pm 0.01	95.95 \pm 0.17	99.97 \pm 0.01	90.58 \pm 0.56	98.67 \pm 0.24
	0.5	95.74 \pm 0.19	99.80 \pm 0.07	95.78 \pm 0.18	99.83 \pm 0.06	84.84 \pm 1.16	93.66 \pm 0.98
	1.0	90.96 \pm 0.72	95.05 \pm 0.65	90.66 \pm 0.79	94.74 \pm 0.71	70.31 \pm 1.76	79.86 \pm 1.51
	2.0	64.62 \pm 1.56	68.78 \pm 1.48	61.25 \pm 1.62	65.34 \pm 1.54	46.65 \pm 1.70	57.43 \pm 1.51
	5.0	30.33 \pm 1.32	35.43 \pm 1.19	28.62 \pm 1.39	33.70 \pm 1.25	24.37 \pm 1.34	37.18 \pm 1.36
L	0.0	96.12 \pm 0.10	99.97 \pm 0.01	96.13 \pm 0.10	99.97 \pm 0.01	93.35 \pm 0.27	99.01 \pm 0.13
	0.5	96.09 \pm 0.10	99.97 \pm 0.01	96.10 \pm 0.10	99.97 \pm 0.01	92.00 \pm 0.35	97.88 \pm 0.23
	1.0	95.41 \pm 0.17	99.26 \pm 0.12	95.51 \pm 0.15	99.37 \pm 0.11	85.29 \pm 0.80	91.42 \pm 0.70
	2.0	75.86 \pm 1.11	79.75 \pm 1.06	73.43 \pm 1.37	77.31 \pm 1.34	57.90 \pm 1.31	65.37 \pm 1.26
	5.0	36.15 \pm 0.97	40.27 \pm 0.92	34.02 \pm 0.92	38.06 \pm 0.89	28.55 \pm 0.84	38.26 \pm 0.89
XL	0.0	96.21 \pm 0.06	99.97 \pm 0.00	96.22 \pm 0.07	99.97 \pm 0.00	96.29 \pm 0.07	99.93 \pm 0.02
	0.5	96.22 \pm 0.07	99.97 \pm 0.00	96.21 \pm 0.06	99.97 \pm 0.00	96.13 \pm 0.07	99.80 \pm 0.04
	1.0	96.20 \pm 0.07	99.97 \pm 0.00	96.19 \pm 0.06	99.97 \pm 0.01	95.26 \pm 0.15	98.97 \pm 0.13
	2.0	88.63 \pm 0.64	92.41 \pm 0.63	85.56 \pm 0.99	89.33 \pm 0.98	77.80 \pm 0.85	81.65 \pm 0.84
	5.0	43.79 \pm 0.70	47.60 \pm 0.68	39.82 \pm 0.86	43.63 \pm 0.83	37.85 \pm 0.59	42.96 \pm 0.57

- [7] A. Agrawal, S. J. Abraham, B. Burger, C. Christine, L. Fraser, J. M. Hoeksema, S. Hwang, E. Travník, S. Kumar, W. Scheirer, J. Cleland-Huang, M. Vierhauser, R. Bauer, and S. Cox, “The next generation of human-drone partnerships: Co-designing an emergency response system,” in *Proceedings of the 2020 CHI Conference on Human Factors in Computing Systems*, ser. CHI ’20. New York, NY, USA: Association for Computing Machinery, 2020, p. 1–13. [Online]. Available: <https://doi.org/10.1145/3313831.3376825>
- [8] R. Yan and A. Julius, “Distributed consensus-based online monitoring of robot swarms with temporal logic specifications,” *IEEE Robotics and Automation Letters*, vol. 7, no. 4, p. 9413–9420, Oct. 2022. [Online]. Available: <http://dx.doi.org/10.1109/LRA.2022.3191236>
- [9] R. K. Ramachandran, P. Pierpaoli, M. Egerstedt, and G. S. Sukhatme, “Resilient monitoring in heterogeneous multi-robot systems through network reconfiguration,” *IEEE Transactions on Robotics*, vol. 38, no. 1, pp. 126–138, 2022.
- [10] O. Shorinwa, R. N. Haksar, P. Washington, and M. Schwager, “Distributed multirobot task assignment via consensus admn,” *IEEE Transactions on Robotics*, vol. 39, no. 3, pp. 1781–1800, 2023.
- [11] M. Braquet and E. Bakolas, “Greedy decentralized auction-based task allocation for multi-agent systems,” 2021. [Online]. Available: <https://arxiv.org/abs/2107.00144>
- [12] A. Prorok, M. A. Hsieh, and V. Kumar, “Fast redistribution of a swarm of heterogeneous robots,” *EAI Endorsed Transactions on Scalable Information Systems*, vol. 3, no. 10, pp. 249–255, 2016.
- [13] J. Liu and R. K. Williams, “Submodular optimization for coupled task allocation and intermittent deployment problems,” *IEEE Robotics and Automation Letters*, vol. 4, no. 4, pp. 3169–3176, 2019.
- [14] B. P. Gerkey and M. J. Matarić, “A formal analysis and taxonomy of task allocation in multi-robot systems,” *The International journal of robotics research*, vol. 23, no. 9, pp. 939–954, 2004.
- [15] G. A. Korsah, A. Stentz, and M. B. Dias, “A comprehensive taxonomy for multi-robot task allocation,” *The International Journal of Robotics Research*, vol. 32, no. 12, pp. 1495–1512, 2013.
- [16] R. M. Zlot, “An auction-based approach to complex task allocation for multirobot teams,” Ph.D. dissertation, Carnegie Mellon University, The Robotics Institute, 2006.
- [17] E. S. Lee, L. Zhou, A. Ribeiro, and V. Kumar, “Graph neural networks for decentralized multi-agent perimeter defense,” *Frontiers in Control Engineering*, vol. 4, Jan. 2023. [Online]. Available: <http://dx.doi.org/10.3389/cteg.2023.1104745>
- [18] Y. Tian, Y. Chang, F. H. Arias, C. Nieto-Granda, J. P. How, and L. Carlone, “Kimera-multi: Robust, distributed, dense metric-semantic slam for multi-robot systems,” *IEEE Transactions on Robotics*, vol. 38, no. 4, 2022.
- [19] W. Luo and K. Sycara, “Minimum k-connectivity maintenance for robust multi-robot systems,” in *2019 IEEE/RSJ International Conference on Intelligent Robots and Systems (IROS)*. IEEE, 2019, pp. 7370–7377.
- [20] W. Luo, S. Yi, and K. Sycara, “Behavior mixing with minimum global and subgroup connectivity maintenance for large-scale multi-robot systems,” in *2020 IEEE International Conference on Robotics and Automation (ICRA)*. IEEE, 2020, pp. 9845–9851.
- [21] C. Lin, W. Luo, and K. Sycara, “Online connectivity-aware dynamic deployment for heterogeneous multi-robot systems,” in *Proceedings of (ICRA) International Conference on Robotics and Automation*, May 2021.
- [22] G. Shi, W. Hönig, Y. Yue, and S.-J. Chung, “Neural-swarm: Decentralized close-proximity multirobot control using learned interactions,” in *2020 IEEE International Conference on Robotics and Automation (ICRA)*. IEEE, 2020, pp. 3241–3247.
- [23] B. Rivière, W. Hönig, Y. Yue, and S.-J. Chung, “Glas: Global-to-local safe autonomy synthesis for multi-robot motion planning with end-to-end learning,” *IEEE Robotics and Automation Letters*, vol. 5, no. 3, pp. 4249–4256, 2020.
- [24] M. Colledanchise, A. Marzotto, D. V. Dimarogonas, and P. Ögren,

- “Adaptive fault tolerant execution of multi-robot missions using behavior trees,” 2015. [Online]. Available: <https://arxiv.org/abs/1502.02960>
- [25] B. Şenbaşlar, W. Hönig, and N. Ayanian, “Rlss: real-time, decentralized, cooperative, networkless multi-robot trajectory planning using linear spatial separations,” *Autonomous Robots*, vol. 47, no. 7, pp. 921–946, 2023.
- [26] R. K. Ramachandran, J. A. Preiss, and G. S. Sukhatme, “Resilience by reconfiguration: Exploiting heterogeneity in robot teams,” in *2019 IEEE/RSJ International Conference on Intelligent Robots and Systems (IROS)*. IEEE, 2019, pp. 6518–6525.
- [27] A. Goeckner, X. Li, E. Wei, and Q. Zhu, “Attrition-aware adaptation for multi-agent patrolling,” *arXiv preprint arXiv:2304.01386*, 2023.
- [28] W. Dai, H. Lu, J. Xiao, Z. Zeng, and Z. Zheng, “Multi-robot dynamic task allocation for exploration and destruction,” *Journal of Intelligent & Robotic Systems*, vol. 98, pp. 455–479, 2020.
- [29] D. Krupke, M. Ernestus, M. Hemmer, and S. P. Fekete, “Distributed cohesive control for robot swarms: Maintaining good connectivity in the presence of exterior forces,” in *2015 IEEE/RSJ International Conference on Intelligent Robots and Systems (IROS)*, 2015, pp. 413–420.
- [30] J. Hudack and J. Oh, “Multi-agent sensor data collection with attrition risk,” in *Proceedings of the International Conference on Automated Planning and Scheduling*, vol. 26, 2016, pp. 166–174.
- [31] A. Halász, M. A. Hsieh, S. Berman, and V. Kumar, “Dynamic redistribution of a swarm of robots among multiple sites,” in *2007 IEEE/RSJ international conference on intelligent robots and systems*. IEEE, 2007, pp. 2320–2325.
- [32] A. Prorok, M. A. Hsieh, and V. Kumar, “Formalizing the impact of diversity on performance in a heterogeneous swarm of robots,” in *2016 IEEE International Conference on Robotics and Automation (ICRA)*. IEEE, 2016, pp. 5364–5371.
- [33] G. Notomista, S. Mayya, S. Hutchinson, and M. Egerstedt, “An optimal task allocation strategy for heterogeneous multi-robot systems,” in *2019 18th European Control Conference (ECC)*. IEEE, 2019, pp. 2071–2076.
- [34] M. R. Pac, A. M. Erkmen, and I. Erkmen, “Control of robotic swarm behaviors based on smoothed particle hydrodynamics,” in *2007 IEEE/RSJ International Conference on Intelligent Robots and Systems*. IEEE, 2007, pp. 4194–4200.
- [35] A.-R. Merheb, V. Gazi, and N. Sezer-Uzol, “Implementation studies of robot swarm navigation using potential functions and panel methods,” *IEEE/ASME Transactions On Mechatronics*, vol. 21, no. 5, pp. 2556–2567, 2016.
- [36] F. Berlinger, M. Gauci, and R. Nagpal, “Implicit coordination for 3d underwater collective behaviors in a fish-inspired robot swarm,” *Science Robotics*, vol. 6, no. 50, p. eabd8668, 2021.
- [37] L. C. Pimenta, G. A. Pereira, N. Michael, R. C. Mesquita, M. M. Bosque, L. Chaimowicz, and V. Kumar, “Swarm coordination based on smoothed particle hydrodynamics technique,” *IEEE Transactions on Robotics*, vol. 29, no. 2, pp. 383–399, 2013.
- [38] L. Sabattini, N. Chopra, and C. Secchi, “Decentralized connectivity maintenance for cooperative control of mobile robotic systems,” *The International Journal of Robotics Research*, vol. 32, no. 12, pp. 1411–1423, 2013.
- [39] N. Michael, M. M. Zavlanos, V. Kumar, and G. J. Pappas, “Maintaining connectivity in mobile robot networks,” in *Experimental Robotics: The Eleventh International Symposium*. Springer, 2009, pp. 117–126.
- [40] M. Cardei and J. Wu, “Energy-efficient coverage problems in wireless ad-hoc sensor networks,” *Computer communications*, vol. 29, no. 4, pp. 413–420, 2006.
- [41] S. Mini, S. K. Udgate, and S. L. Sabat, “M-connected coverage problem in wireless sensor networks,” *International scholarly research notices*, vol. 2012, no. 1, p. 858021, 2012.
- [42] J. Scherer and B. Rinner, “Multi-robot persistent surveillance with connectivity constraints,” *IEEE Access*, vol. 8, pp. 15 093–15 109, 2020.
- [43] Y. Wang, Y. Wang, Y. Cao, and G. Sartoretti, “Spatio-temporal attention network for persistent monitoring of multiple mobile targets,” in *2023 IEEE/RSJ International Conference on Intelligent Robots and Systems (IROS)*. IEEE, 2023, pp. 3903–3910.
- [44] K. Su and F. Qian, “Multi-uav cooperative searching and tracking for moving targets based on multi-agent reinforcement learning,” *Applied Sciences*, vol. 13, no. 21, p. 11905, 2023.
- [45] H. Kesten, “Percolation theory for mathematicians,” *Progress in Probability and Statistics*, vol. 2, 1982.
- [46] I. Balberg, “Continuum percolation,” *Encyclopedia of Complexity and Systems Science*, pp. 1443–1475, 2009.
- [47] S. Torquato, *Random heterogeneous materials: microstructure and macroscopic properties*. Springer Science & Business Media, 2002.
- [48] G. Grimmett, *Percolation*, 2nd ed. Springer-Verlag Berlin Heidelberg, 1999.
- [49] K. Zhang, Z. Yang, and T. Başar, “Multi-agent reinforcement learning: A selective overview of theories and algorithms,” *Handbook of Reinforcement Learning and Control*, pp. 321–384, 2021.
- [50] J. Foerster, I. A. Assael, N. De Freitas, and S. Whiteson, “Learning to communicate with deep multi-agent reinforcement learning,” *Advances in neural information processing systems*, vol. 29, 2016.
- [51] J. Chen and X. Ran, “Deep learning with edge computing: A review,” *Proceedings of the IEEE*, vol. 107, no. 8, pp. 1655–1674, 2019.
- [52] S. He, S. Han, S. Su, S. Han, S. Zou, and F. Miao, “Robust multi-agent reinforcement learning with state uncertainty,” *arXiv preprint arXiv:2307.16212*, 2023.
- [53] J. K. Gupta, M. Egorov, and M. Kochenderfer, “Cooperative multi-agent control using deep reinforcement learning,” in *Autonomous Agents and Multiagent Systems: AAMAS 2017 Workshops, Best Papers, São Paulo, Brazil, May 8-12, 2017, Revised Selected Papers 16*. Springer, 2017, pp. 66–83.
- [54] S. Omidshafiei, J. Papis, C. Amato, J. P. How, and J. Vian, “Deep decentralized multi-task multi-agent reinforcement learning under partial observability,” in *International Conference on Machine Learning*. PMLR, 2017, pp. 2681–2690.
- [55] K. Nguyen, S. Schoedel, A. Alavilli, B. Plancher, and Z. Manchester, “Tnympc: Model-predictive control on resource-constrained microcontrollers,” in *2024 IEEE International Conference on Robotics and Automation (ICRA)*. IEEE, 2024, pp. 1–7.
- [56] Y. Song, A. Romero, M. Müller, V. Koltun, and D. Scaramuzza, “Reaching the limit in autonomous racing: Optimal control versus reinforcement learning,” *Science Robotics*, vol. 8, no. 82, p. eadg1462, 2023.